# This is the accepted manuscript of the contribution published as:

Schweizer, S.A., Hoeschen, C., **Schlüter, S.**, Kögel-Knabner, I., Mueller, C.W. (2018): Rapid soil formation after glacial retreat shaped by spatial patterns of organic matter accrual in microaggregates *Glob. Change Biol.* **24** (4), 1637 – 1650

# The publisher's version is available at:

http://dx.doi.org/10.1111/gcb.14014

#### MR. STEFFEN A. SCHWEIZER (Orcid ID : 0000-0002-9489-1005)

Article type : Primary Research Articles

Rapid soil formation after glacial retreat shaped by spatial patterns of organic matter accrual in microaggregates

Running head: Soil organic matter accrual at microscale

Steffen A. Schweizer<sup>1</sup>\*, Carmen Hoeschen<sup>1</sup>\*, Steffen Schlüter<sup>2</sup>, Ingrid-Kögel-Knabner<sup>1, 3</sup>, and Carsten W. Mueller<sup>1</sup>

<sup>1</sup> Chair of Soil Science, TUM School of Life Sciences Weihenstephan, Technical University of Munich, Emil-Ramann-Str. 2, 85354 Freising-Weihenstephan, Germany

<sup>2</sup> Department of Soil System Sciences, Helmholtz-Centre for Environmental Research - UFZ, Theodor-Lieser-Straße 4, 06120 Halle (Saale), Germany

<sup>3</sup> Institute for Advanced Study, Technical University of Munich, Lichtenbergstraße 2a, 85748 Garching,

Germany

Correspondence: Steffen Schweizer, phone +49 8161 71-4206, fax +49 8161 71 -4466, email

schweizer@wzw.tum.de

<sup>\*</sup> These authors contributed equally to this work.

Keywords: soil carbon sequestration, glacier forefield, mineral-associated organic matter, organomineral associations, organic coating, biogeochemical soil interfaces, spatial complexity, NanoSIMS

Type of paper: primary research article

This article has been accepted for publication and undergone full peer review but has not been through the copyediting, typesetting, pagination and proofreading process, which may lead to differences between this version and the Version of Record. Please cite this article as doi: 10.1111/gcb.14014 This article is protected by copyright. All rights reserved.

Global change contributes to the retreat of glaciers at unprecedented rates. The deglaciation facilitates biogeochemical processes on glacial deposits with initiating soil formation as an important driver of evolving ecosystems. The underlying mechanisms of soil formation and the association of soil organic matter (SOM) with mineral particles remain unclear, although further insights are critical to understand carbon sequestration in soils. We investigated the microspatial arrangement of SOM coatings at intact soil microaggregate structures during various stages of ecosystem development from 15 to >700 years after deglaciation in the proglacial environment of the Damma glacier (Switzerland). The functionally important clay-sized fraction (<2  $\mu$ m) was separated into two density fractions with different amounts of organo-mineral associations: light (1.6-2.2 g cm<sup>-3</sup>) and heavy  $(>2.2 \text{ g cm}^{-3})$ . To quantify how SOM extends across the surface of mineral particles (coverage) and if SOM coatings are distributed in fragmented or connected patterns (connectivity), we developed an image analysis protocol based on nanoscale secondary ion mass spectrometry (NanoSIMS). We classified SOM and mineral areas depending on the <sup>16</sup>O<sup>-</sup>, <sup>12</sup>C<sup>-</sup>, and <sup>12</sup>C<sup>14</sup>N<sup>-</sup> distributions. With increasing time after glacial retreat, the microspatial coverage and connectivity of SOM increased rapidly. The rapid soil formation led to a succession of patchy distributed to more connected SOM coatings on soil microaggregates. The maximum coverage of 55 % at >700 years suggests direct evidence for SOM sequestration being decoupled from the mineral surface, as it was not completely masked by SOM and retained its functionality as an ion exchange site. The chemical composition of SOM coatings showed a rapid change towards a higher CN:C ratio already at 75 years after glacial retreat, which was associated with microbial succession patterns reflecting high N assimilation. Our results demonstrate that rapid SOM sequestration drives the microspatial succession of SOM coatings in soils, a process that can stabilize SOM for the long-term.

# Introduction

Global warming and altered precipitation patterns change polar and alpine ecosystems at unprecedented progression (Ernakovich et al., 2014), accelerating the retreat of glaciers and exposing new surface for soil formation. In the Alps, the glacier area is estimated to have decreased by 30-50 % from 1850 to 2000 (Haeberli & Beniston, 1998; Zemp et al., 2006). With ongoing glacial retreat, the proglacial soil development was shown to occur at a decadal to centennial timescale with rapid progress during the first decades (Egli et al., 2010; He & Tang, 2008). The exposure of glacier forefields provides sites that are appropriate ecological chronosequences at all scales of soil development through space-for-time substitution (Huggett, 1998; Walker et al., 2010). After deglaciation, the glacial deposits undergo more pronounced geochemical weathering and alteration processes leading to the presence of phyllosilicates and (hydr-)oxides in the fine particle fraction (Anderson, 2007; Kiczka et al., 2011). The deposits are rapidly colonized by soil biota and plants supplying organic matter (Conen et al., 2007). This leads to the formation of organo-mineral associations, which play a major role in the stabilization of soil organic matter (SOM) (Chenu & Stotzky, 2002; Conant et al., 2011; Dümig et al., 2012; von Lützow et al., 2006). Especially clay-sized particles like clay minerals and pedogenic oxides foster the sequestration and have the highest potential capacity to stabilize SOM (Kögel-Knabner et al., 2008; Pronk et al., 2012). Previous studies were focused on empiric relationships between SOM and biogeochemical properties at bulk scale and did not consider spatial heterogeneity within the newly formed soil microstructures. Nevertheless, the analysis of SOM arrangement at the microscale is of critical importance for our understanding of how initial soils accumulate SOM in soil structures that can stabilize organic carbon in the long-term.

The analysis of intact soil structures has revealed that SOM is distributed heterogeneously on biogeochemical interfaces rather than a homogeneous extensive monolayer coating (Chenu & Plante, 2006; Vogel *et al.*, 2014; Dignac *et al.*, 2017). The underlying factors for the complex microspatial arrangement of SOM on mineral surfaces are thought to be the heterogeneous distribution of various physicochemical soil properties like the access to fine mineral surface (Kleber This article is protected by copyright. All rights reserved.

*et al.*, 2015; Dignac *et al.*, 2017; Totsche *et al.*, 2018). Previous bulk and surface analyses suggested that SOM accumulates as discrete patches occluding mineral surfaces and topographies with high surface area (Kaiser & Guggenberger, 2007; Wagai *et al.*, 2009). In a recent study with direct measurement of SOM coverages at intact soil microaggregates and primary clay-sized particles, Vogel *et al.* (2014) observed preferential retention of new SOM at already existing organo-mineral associated SOM. Most microbial-derived SOM is contained in the fine-sized soil particle fractions that indicate higher surface areas than coarser particles facilitating the attachment and protection of microorganisms in the fine fraction (Kögel-Knabner *et al.*, 2008). Microorganisms can colonize the soil volume in patchy distributed microenvironments, forming microbial hotspots, and interact with the mineral particles (Grundmann, 2004; Kim *et al.*, 2015; Nunan *et al.*, 2007). Given the complex spatial arrangement of SOM, it is crucial to investigate intact microstructures at the relevant scale to understand the mechanisms of SOM accrual in new developing systems.

In addition to the spatial scale, the temporal development in the surrounding ecosystem could influence SOM accrual and composition during soil formation. Ecosystems in proglacial and comparable environments were postulated to develop in three successional stages on a decadal to centennial timescale (Ollivier *et al.*, 2011; Schulz *et al.*, 2013). At the initial stage, barren deposits, scarce vegetation, and limited nutrient availability lead to the selection of autotrophic microorganisms and those associated with mineral weathering (Bradley *et al.*, 2014; Schmidt *et al.*, 2008; Zumsteg *et al.*, 2012). The accumulation of C and N is considered low at the initial stage and increases with the establishment of vegetation and associated microbes contributing to N assimilation (Esperschütz *et al.*, 2011; Hämmerli *et al.*, 2007; Zumsteg *et al.*, 2012). At this intermediate stage, both plants and soil microorganisms indicate high N demands (Ollivier *et al.*, 2011). At a later stage, N is mostly derived from the biomass and nitrification, denitrification, as well as mineralization processes become more active (Brankatschk *et al.*, 2011; Ollivier *et al.*, 2011; Tscherko *et al.*, 2004).

The aim of this study was to investigate whether the initial soil structure formation is driven by successive patterns of microscale SOM coverage considering both the microspatial heterogeneity and This article is protected by copyright. All rights reserved.

the temporal development of SOM accrual. We investigated the sequestration of SOM by formation of coatings on soil mineral surfaces within a chronosequence in the forefield of the Damma glacier (Switzerland) including various ecosystem development stages at 15 to >700 years after glacial retreat (Bernasconi et al., 2011; Dümig et al., 2011). Advanced spectromicroscopic techniques allow for promising observations of soil processes at micro/submicroscale (Rennert et al., 2012). Using nanoscale secondary ion mass spectrometry (NanoSIMS) enables the spatial measurement of up to seven ion species simultaneously at a lateral resolution of approximately 100 nm (Herrmann et al., 2007; Mueller et al., 2013). In our study, the secondary ion distributions of <sup>16</sup>O<sup>-</sup> (indicative for soil particles) as well as  ${}^{12}C^{-}$  and  ${}^{12}C^{14}N^{-}$  (indicative for SOM) were used to analyze the soil formation and spatial relationships of SOM accrual on mineral surfaces. To describe the spatial arrangement of SOM at the microscale, we developed an image analysis protocol using supervised pixel classification with a machine-learning algorithm based on the secondary ion distributions (particle and coating size, SOM coverage and connectivity). Our automatic image analysis based on NanoSIMS measurements provided for the first time a spatial quantification of developing SOM coatings and their C and N composition in a long-term dataset of environmental samples. This approach allowed us to identify spatial patterns of soil microstructure formation that are dominating sites for long-term SOM sequestration and cycling as well as microbial activity on freshly exposed land affected by global change.

#### Materials and methods

#### Research site sampling, fractionation, and bulk soil analyses

The soil samples originate from a chronosequence study in the foreland of the Damma glacier in Switzerland (Dümig *et al.*, 2012). The mean annual temperature at the research site is 2.2 °C and the mean annual precipitation is about 2300-2400 mm mostly falling as snow (Dümig *et al.*, 2011; Smittenberg *et al.*, 2012). The soils in the forefield of the Damma glacier developed on deposited granite of the Aare Massif, metamorphosed under greenschist facies conditions after the discontinuous retreat of the glacier (Bernasconi *et al.*, 2011; Keusen *et al.*, 1989; Schaltegger, 1990). This article is protected by copyright. All rights reserved. Dümig et al. (2012) sampled triplicates from four development stages that were classified according to the time after glacial retreat: young (15 years), intermediate (71 years, 79 years), old (111 years), and a mature reference site located outside the forefield (>700 years) (Bernasconi et al., 2011). We chose five soil samples from all development stages of the work of Dümig et al. (2012). The time after glacial retreat for the young and intermediate soils was determined based on glacial movement records. For the old and mature soil, the time after glacial retreat was estimated with records of neighboring glaciers. More details about the retreat history of the Damma glacier are described by Bernasconi et al. (2011). We used clay-sized fractions extracted from the bulk soil within 0-5 cm soil depth with a combined size and density fractionation by Dümig *et al.* (2012). Briefly, the >1.6 g cm<sup>-3</sup> mineral-associated fraction after suspension in sodium polytungstate solution was dispersed with 200 J ml<sup>-1</sup> (Branson Sonifier 250). Afterwards, the clay-sized fraction (<2  $\mu$ m) was extracted by sedimentation, recovered by pressure filtration (0.45 µm; CN), and freeze-dried. To separate fractions with differing amounts of organo-mineral associations (Hatton et al., 2012; Sollins et al., 2009), we additionally fractionated the mineral-associated clay-sized fraction (>1.6 g cm<sup>-3</sup>) into a light fraction (1.6-2.2 g cm<sup>-3</sup>) and a heavy fraction (>2.2 g cm<sup>-3</sup>) by density fractionation using sodium polytungstate. We analyzed the concentration of organic C and total N in the light and heavy claysized fractions through dry combustion using a CN analyzer (Vario EL, Elementar).

# Microscale element distribution measured with NanoSIMS analyses

We applied the soil clay-sized fractions on a Si wafer as  $1 \text{ g l}^{-1}$  water suspension and dried them in the desiccator at room temperature (Mueller *et al.*, 2012). On all samples, representative areas containing both smaller primary particles and larger organo-mineral associations were chosen using secondary electron microscopy (SEM) (Fig. S1a). The SEM analyses were conducted with a low vacuum SEM with a tungsten cathode using 15 keV (Jeol JSM 5900). Prior to SEM and NanoSIMS, we coated the samples under Ar atmosphere with 5 nm Au and ~30 nm Au/Pd, respectively. On each sample, 8-26 areas were analyzed with NanoSIMS 50L (Cameca, Gennevilliers, France) (Fig. S1b) resulting in 121 measurements in total. We used a Cs<sup>+</sup> primary ion beam with 16 keV primary ion This article is protected by copyright. All rights reserved. impact energy while simultaneously recording secondary ion distributions for <sup>12</sup>C<sup>-</sup>, <sup>16</sup>O<sup>-</sup>, and <sup>12</sup>C<sup>14</sup>N<sup>-</sup> (in addition, <sup>30</sup>Si<sup>-</sup>, <sup>32</sup>S<sup>-</sup>, <sup>27</sup>Al<sup>16</sup>O<sup>-</sup>, and <sup>56</sup>Fe<sup>16</sup>O<sup>-</sup> distributions were measured but are not shown here). The areas were pre-sputtered with a high Cs<sup>+</sup> ion beam to remove surface contamination as well as Au/Pd coating and to implant reactive Cs<sup>+</sup> ions into the sample increasing the secondary ion yield until a steady state of secondary ions was reached. Depending on the size of particles, the field of view was 30x30 µm with pixel dimensions of 256x256 pixels and a dwell time of 30 ms or a field of view of 40x40 µm with 512x512 pixels and 10 ms dwell time. The NanoSIMS electron flood gun was used to compensate for charging effects on soil mineral particles.

#### Multi-channel machine-learning segmentation and image analysis

The NanoSIMS measurements (n=121) were corrected for electron multiplier dead-time (44 ns) using the OpenMIMS plugin for ImageJ (Gormanns et al., 2012). To avoid distortion due to outlying pixels, we enhanced the image contrast of each ion distribution by setting the darkest (brightest) 0.5% percentile of pixels to the minimum (maximum) gray value and linear stretching of the remaining pixels to the full 16-bit range by employing the contrast enhancement tool in the Fiji package for ImageJ (Schindelin et al., 2015). With these images, we performed a supervised pixel classification of the <sup>16</sup>O<sup>-</sup>, <sup>12</sup>C<sup>-</sup>, and <sup>12</sup>C<sup>14</sup>N secondary ion distributions (Fig. S1b-g) using the machinelearning algorithm implemented in Ilastik 1.2 (Sommer et al., 2011). The <sup>16</sup>O<sup>-</sup> ion distribution was used to differentiate between the sample (soil particles) and the Si wafer. For the sample particles, the <sup>12</sup>C<sup>-</sup> and <sup>12</sup>C<sup>14</sup>N<sup>-</sup> ion distributions were used to segment the area into mineral particle surface and SOM coating (Hatton et al., 2012, Remusat et al., 2012, Vogel et al., 2014). Multiple image features like intensity, gradient, and texture at various spatial scales in all three ion distributions served as input information for the machine-learning algorithm. The NanoSIMS images were segmented into background, mineral particle surface, and SOM coatings according to manually identified training data for each material class that covered less than 1 % of the image area (Fig. S1c, further details in the supporting information). During the training of the image analysis, we used maps of relative uncertainty of the machine-learning algorithm (Fig. S1d) to detect ambiguous image areas. We This article is protected by copyright. All rights reserved.

assigned further training lines until areas of relatively higher uncertainty were confined to the borders of the assigned segmentation classes (Fig. S1d). We use the term soil particles to refer to both primary particles and aggregates in this study.

We used the segmented images to compute measures of the spatial arrangement of SOM coatings for each particle (Fig. S1i). In total, 2448 particles were detected, 1013 of them coated with 4668 individual coatings across all 121 images (Table S1). The particle area comprises the total area of both the mineral and the associated SOM coating. Particles smaller than 0.05  $\mu$ m<sup>2</sup> (4-8 pixel<sup>2</sup>) were excluded for further calculations. We computed the mean particle size and SOM coating size based on the projected image areas for each density fraction and time after glacial retreat. The frequency distribution of particles was evaluated for several size classes <1  $\mu$ m<sup>2</sup>, 1-5  $\mu$ m<sup>2</sup>, 5-10  $\mu$ m<sup>2</sup>, 1-50  $\mu$ m<sup>2</sup>, and >50  $\mu$ m<sup>2</sup>. Previous SEM analyses of clay-sized fraction (<2  $\mu$ m) obtained by sedimentation has shown that these fractions regularly exhibit much larger diameters due to the non-spherical platy structure of clay particles and varying densities due to associated SOM (Konert & Vandenberghe, 1997). Regarding the size of the SOM coatings, we reported the frequency distribution for the size classes <0.5  $\mu$ m<sup>2</sup>, 0.5-2  $\mu$ m<sup>2</sup>, 2-5  $\mu$ m<sup>2</sup>, 5-20  $\mu$ m<sup>2</sup>, and >20  $\mu$ m<sup>2</sup>.

The coverage of mineral particles with SOM coatings (SOM coverage) was calculated as the proportion of the SOM coating area from the total particle area of both mineral particle and SOM coating segments. The total coverage  $\overline{C}$  of each density fraction, time after glacial retreat, and respective size class was computed as

$$\bar{C} = \frac{\sum_{i=1}^{N_{par}} \sum_{j=1}^{N_{som}} O_{ij}}{\sum_{i=1}^{N_{par}} P_i}$$
(1)

where  $N_{par}$  denotes the number of particles with label *i*,  $N_{SOM}$  denotes the number of organic coatings with label *j*,  $O_{ij}$  denotes the size of an individual SOM coating [ $\mu$ m<sup>2</sup>], and  $P_i$  denotes the size of a particle [ $\mu$ m<sup>2</sup>].

We used the SOM coatings to calculate the connectivity per particle (SOM coating connectivity). For every particle with label *i*, the dimensionless connectivity indicator  $\Gamma_i$  (Renard & Allard, 2013; Schlüter *et al.*, 2014) of the corresponding SOM coatings was computed as

$$\Gamma_{i} = \frac{\sum_{j=1}^{N_{SOM}} (O_{ij}^{2})}{\left[\sum_{j=1}^{SOM} O_{ij}\right]^{2}}$$
(2)

Hence, the SOM coating connectivity  $\Gamma_i = 1$  for a single, fully connected SOM coating on one particle, whereas  $\Gamma_i \rightarrow 0$  for patchy structures with many isolated SOM coatings on the same particle. To account for the varying particles sizes, we reported the average connectivity as an areaweighted mean (Schumaker, 1996) according to

$$\bar{\Gamma} = \sum_{i=1}^{N_{par}} \left( \frac{O_i \Gamma_i}{\sum_{i=1}^{N_{par}} O_i} \right)$$
(3)

To analyze the relative chemical composition of the SOM coatings, we computed the normalized CN:C ratio ( ${}^{12}C^{14}N^-$ : ( ${}^{12}C^{14}N^-$  +  ${}^{12}C^-$ )) between secondary ion distributions for each SOM coating without any contrast enhancement (Fig. S1k). A ratio <0.5 indicates relative C-rich SOM coatings with more C than N, whereas a ratio >0.5 indicates relative N-rich SOM coatings with more N than C. The CN:C ratio was reported as an arithmetic mean across the density fraction, time after glacial retreat, and respective size class. A linear relationship was demonstrated for mean  ${}^{12}C^{14}N^-$ :  ${}^{12}C^-$  and  ${}^{12}C^{14}N^-$ :  ${}^{12}C_2^-$  ratios obtained by NanoSIMS and C:N ratios measured at bulk scale by an elemental analyzer (Alleon *et al.*, 2015; Hatton *et al.*, 2012).

We used RStudio 0.99 (RStudio Team, 2015) to compile the results of the image analysis and compute averages and standard errors for the spatial measures. The spatial measures were tested for normal distribution and homogeneity of variances. To test the effect of time after glacial retreat on particle sizes, SOM coating sizes, and the elemental ratios, we used a one-way ANOVA and Tukey's honest significant difference test to compute pairwise differences of means.

#### Results

# Bulk soil organic carbon concentration and change of the mass contribution of heavy and light density clay-sized fractions

In the clay-sized fraction of the initially forming soils, the soil organic carbon (SOC) concentration increased rapidly over time after glacial retreat from the young (15 years) to the intermediate and old soil stages (75 years, 111 years) and still experienced an additional increase in the mature reference soil (Table 1). The SOC concentrations of the intermediate and old soil stages showed a variability that is attributed to the heterogeneity of the glacial forefield. Within the heavy clay-sized fraction (>2.2 g cm<sup>-3</sup>), the SOC concentration increased with time after glacial retreat in the initial stages, whereas it decreased at the mature site (>700 years). Within the light clay-sized fraction (1.6-2.2 g cm<sup>-3</sup>), the SOC concentration was twice the one in earlier soil development stages except the mature site where the SOC concentration was higher in the light clay-sized fraction than in the heavy clay-sized fraction. The average bulk C:N ratio in the light fraction was 2 units (22 %) higher than in the heavy fraction (Table 1). In the light fraction, the C:N ratio was higher in the young and mature soil (15 and >700 years) than in the intermediate and old soils (Table 1).

Concurrent with increasing SOC concentration, we observed a rapid change in the mass proportions of the two clay-sized density fractions: With increasing time after glacial retreat, the majority of the particle mass was recovered in the light fraction while the contribution of the heavy fraction decreased (Fig. 1a). At 111 years after glacial retreat, the contributions of heavy and light clay-sized fractions were similar, whereas at >700 years the contribution of the light fraction was predominant (Fig. 1a). The soil at 79 years indicated a higher clay content than the other samples leading to a higher mass contribution of the clay-sized fractions to the bulk soil (Fig. 1a). The SOC concentration of the clay-sized fractions normalized to the bulk soil increased over time except for the old soil stage (111 years) (Fig. 1b).

#### Spatial arrangement of soil microaggregates analyzed by NanoSIMS

The NanoSIMS measurements revealed the spatial distribution of SOM coatings ( ${}^{12}C$ ,  ${}^{12}C^{14}N$ ) and mineral particles ( ${}^{16}O$ ) at the microscale. Exemplary NanoSIMS measurements show a high heterogeneity (Fig. 2). Some mineral particles were partially covered by SOM coatings and some mineral particles were without coatings or fully coated (Fig. 2). We observed a rapid increase of the area covered by SOM coatings on microscale particles, that were composed of individual mineral particles or microaggregates upon glacial retreat. In the heavy clay-sized fraction (>2.2 g cm<sup>-3</sup>), most particles appeared to have a plain, smooth surface, and over time some microaggregates entangled by SOM were observed (Fig. 2a, b). In contrast to the heavy fraction, in the light clay-sized fraction (1.6-2.2 g cm<sup>-3</sup>) numerous microaggregates appeared at all soil development stages (Fig. 2c). In both clay-sized density fractions, we found a high heterogeneity in the size of particles and SOM coatings (Fig. 2). The distribution of  ${}^{12}C$  and  ${}^{12}C^{14}N^{-}$  also indicated a high heterogeneity in the chemical composition of the SOM coatings, showing both C-rich and N-rich SOM coatings in the same measurement (Fig. 2).

#### Sizes of particles and SOM coatings provided by image analysis

A quantification of the spatial arrangement of soil minerals and SOM coatings at the microscale was obtained by multi-channel machine-learning segmentation and image analysis. The size of the individual particles evolved differently in both clay-sized density fractions: The mean particle size in the heavy fraction increased over time (Fig. 3a), whereas it decreased in the light fraction (Fig. 3b). Both the light and heavy fraction only reach comparable average particle sizes in the mature soil (>700 years) (Fig. 3a, b). On average, 73 % of particles were <5  $\mu$ m<sup>2</sup> in both density fractions. The relative frequency of >50  $\mu$ m<sup>2</sup> increased in the heavy fraction, whereas in the light fraction, the frequency of particles 10-50  $\mu$ m<sup>2</sup> increased at the expense of the particles >50  $\mu$ m<sup>2</sup> (Fig. 3a, b).

The SOM coating size was consistently higher in the light clay-sized fraction than in the heavy fraction at all development stages (Fig. 3c, d). On average, 54 % of SOM coatings were <0.5  $\mu$ m<sup>2</sup> in the light fraction and 68 % were that small in the heavy fraction (Fig. 3c, d). SOM coatings were This article is protected by copyright. All rights reserved.

smallest in the young soil (15 years) and increased in both heavy and light fraction over time. In the heavy fraction, the SOM coating size was smaller in the young soil (15 years) than in the old soil (111 years), and the other stages were in between (Fig. 3c). In the light fraction, the SOM coating size increased from an average size of  $1 \mu m^2$  to  $7 \mu m^2$  from the young soil (15 years) to the mature soil (>700 years) (Fig. 3d). A higher variability of both particle and SOM coating sizes in the light fraction compared to the heavy fraction was found (Fig. 3).

#### Coverage of soil organic matter on mineral surfaces provided by image analysis

Based on the image analysis using the elemental distributions by NanoSIMS, we computed the degree of coverage of the total mineral area with the total area of SOM coatings (Fig. 4). The SOM coverage increased with time after glacial retreat in the light clay-sized fraction (Fig. 4b): The SOM coverage was higher in the intermediate and old soils (71, 79, and 111 years) and still higher in the mature soil (>700 years) than the earlier soil development stages. At the young soil, 9 % of the mineral surface was covered, whereas at the mature site, SOM coverage of 56 % was reached in the light clay-sized fraction (Fig. 4b), which dominated the mass contribution at that time (Fig. 2). In contrast, the SOM coverage in the heavy clay-sized fraction was higher in the old soil than in the mature soil, which also had the highest bulk SOC concentration (Fig. 4a, Table 1).

The coverage of 0-5  $\mu$ m<sup>2</sup> particles was higher in the heavy clay-sized fraction of the mature soil than the larger particles (Fig. 4a). In contrast, the coverage of the >10  $\mu$ m<sup>2</sup> particles in the light fraction was higher than the coverage of smaller particles in the intermediate, old, and mature soil (Fig. 4b). This means that the larger particles contributed more to the increasing coverage in the light fraction than in the heavy fraction.

# Connectivity of soil organic matter coatings on individual particles provided by image analysis

To evaluate the development of the spatial arrangement of the SOM coatings over time, we computed their connectivity on the individual particles (Fig. 5). In the light clay-sized fraction, we found an increase of the area-weighted mean SOM connectivity with time after glacial retreat This article is protected by copyright. All rights reserved.

(Fig. 5b). The SOM connectivity of the young and intermediate sites (15 and 75 years) was in a similar range (Fig. 5b).

The connectivity of the SOM coatings in the heavy clay-sized fraction was higher than the one of the light fraction at the young soil, which coincides with the heavy fraction having the major mass contribution to the bulk soil (Fig. 5a, Fig. 2). Over time, the SOM connectivity decreased from 0.43 to 0.25 in the heavy fraction (Fig. 5a). In the mature soil, the SOM connectivity decreased with increasing particle sizes in the heavy fraction (Fig. 5a). However, in the light fraction of the mature soil, the SOM connectivity increased with increasing particle sizes (Fig. 5b).

#### C and N composition of soil organic matter coatings provided by image analysis

The normalized element ratio of  ${}^{12}C^{14}N^{-}$  and  ${}^{12}C^{-}$  was used to track changes in the C and N composition of SOM coatings during soil formation. The average CN:C ratio of the light clay-sized fraction was 0.1 units higher (23 %) than the one of the heavy fraction (Fig. 6). In the light clay-sized fraction, the CN:C was higher at the intermediate soil (75 years) than at the young and old soil (15 years, 111 years) (Fig. 6b). In the mature soil (>700 years), the CN:C ratio was higher in the heavy clay-sized fraction than in the light fraction (Fig. 6). In the heavy fraction, the CN:C ratio was higher in the heavy clay-sized fraction than in the light fraction (Fig. 6). In the heavy fraction, the CN:C ratio was higher for larger SOM coating sizes except >20  $\mu$ m<sup>2</sup> at 79 and 111 years (Fig. 6a). In contrast, the CN:C ratio in the light fraction remained similar for all SOM coating sizes (Fig. 6b).

#### Discussion

#### Microspatial soil formation through the accrual of organic matter

After the retreat of the Damma glacier, SOM rapidly associated with a fine mineral surface and formed soil microaggregates. The increase of the mass contribution of the light clay-sized fraction (1.6-2.2 g cm<sup>-3</sup>) at the expense of the heavy fraction (>2.2 g cm<sup>-3</sup>) with time after glacial retreat indicates that the sequestration of SOM on mineral surfaces occurred more rapidly than the development of a fresh mineral surface through the weathering of the glacial deposits (Fig. 1). In the geomorphologic active glacier forefield, the particularly high clay content of the soil at 79 years This article is protected by copyright. All rights reserved.

points to a difference in the deposition of glacial till and subsequent glaciofluvial erosion and deposition at that time stage. Previous studies in comparable environments also found variable soil texture without a chronological trend in proglacial environments (Conen *et al.*, 2007; Dümig *et al.*, 2011). Therefore, the increasing recovery of particles in the light fraction over time was rather linked to the accrual of SOM that contributes to a lower specific weight. This corroborates previous studies at the bulk scale that suggested that the SOM input from the establishing vegetation and an increase of biological activity as well as the SOM accumulation in the soil were higher than the supply of adsorptive mineral surfaces from mineral weathering (Dümig *et al.*, 2012; Schulz *et al.*, 2013). Our results provide direct evidence at the microscale for the hypothesis that the increased surface area cannot be supplied at the same rate through mineral weathering as shown by X-ray diffraction analyses on the same samples as this study (Dümig *et al.*, 2012), which reported biotite weathering to hydrobiotite at a low degree.

The SOC concentration of the clay-sized fraction increased within several decades and was related to an increase in the coverage of SOM coatings on mineral surfaces (Table 1, Fig. 1b, Fig. 4). This means that the sequestration of SOM on mineral surfaces drives a growth of associated SOM coatings at a decadal timescale. In addition, the increase of the connectivity of SOM coatings on the individual particles at centennial timescale (111 and >700 years after glacial retreat) (Fig. 5) demonstrates that the increased SOM coating size and coverage is related to the growth of already existing SOM coatings. This means that SOM coatings grow together instead of binding at new spots that are not connected to existing coatings. This finding confirms the concept of SOM being associated with mineral surfaces as patchy coatings (Dignac et al., 2017; Wagai et al., 2009) and that these existing coatings act as preferential spots for the retention of fresh SOM substrate as found previously by a spatial analysis of <sup>13</sup>C-labelled litter (Vogel et al., 2014). The preferential sorption of SOM to organic surfaces was explained by a more readily sorption through peptide binding and ligand exchange than unconditioned mineral surfaces (Sollins et al., 2006; Kleber et al., 2015). Other studies have connected the in-situ accrual of SOM to the growth of bacterial patches that occurs due to chemotactically driven cell movement and dormancy during nutrient limitation (Grundmann, This article is protected by copyright. All rights reserved.

2004; Kim *et al.*, 2015; Pallud *et al.*, 2004). The increased abundance of microorganisms during the ecosystem development over time after glacial retreat (Schulz *et al.*, 2013) and the predominant abundance of bacteria in the fine soil fractions (Kögel-Knabner *et al.*, 2008) suggest that microbial mechanisms could enhance the growth of already existing SOM coatings.

Our NanoSIMS image analysis revealed that the SOM coverage did not exceed 32 % at the old soil and was 56 % at the mature site (Fig. 4). This means that 68 % and 44 % of the soil particle surfaces remained uncovered in the forefield and at the mature site, respectively. Through the application of the clay-sized fraction as suspension onto Si wafers, we were able to directly observe the mineral surfaces covered with SOM at intact soil microstructures. A previous NanoSIMS image analysis guantified the SOM coverage as <19% in the ploughed topsoil of a Luvisol (Vogel et al., 2014) which is comparable to the SOM coverage of the intermediate soil in this study. Another NanoSIMS image analysis quantified the SOM coverage as 57 % in the 1.85-2.0 g cm<sup>-3</sup> fraction and as <31 % in the >2.2 g cm<sup>-3</sup> fraction (Hatton *et al.*, 2012). In accordance with Hatton *et al.* (2012), our image analysis also revealed higher SOM coverages in the light clay-sized fraction (1.6-2.2 g cm<sup>-3</sup>) than the one in the heavy fraction (>2.2 g cm<sup>-3</sup>) at the oldest mature site (700 years) (Fig. 4). This implies that the total surface area of the fine-sized fraction is not decisive for the accumulation and preservation of organic carbon associated with minerals. Such decoupling of SOM sequestration from mineral surface properties provides direct evidence for the findings at bulk scale in earlier work in which higher carbon sequestration in a clay loam soil was found than as expected from established carbon sequestration models (Yang et al., 2016). Instead, the differential surface properties of both mineral and organic surfaces determining the association with SOM should be considered in conceptual models of soil carbon sequestration. The coverage of mineral surface with SOM coating mostly retained the functionality as an ion exchange site of mineral particles because their surface is not completely coated. This suggests that properties of the SOM do rather add to the mineral properties instead of replacing them concerning soil ecological functions like the important interactions with microbial activity and nutrient retention.

Through density fractionation of the clay-sized fraction, we could observe distinct compositions of organo-mineral associations in the two density fractions. The  $<1 \mu m^2$  particles in the heavy claysized fraction (>2.2 g cm<sup>-3</sup>) were covered to a higher extent with SOM than the >1  $\mu$ m<sup>2</sup> particles at 111 and >700 years (Fig. 4a). In the light clay-sized fraction (1.6-2.2 g cm<sup>-3</sup>), however, the >10  $\mu$ m<sup>2</sup> particles were covered to a higher extent than the smaller particles at 111 and >700 years (Fig. 4b). We observed similar trends for the connectivity of the SOM coatings on particles of various sizes (Fig. 5). The observation of different relationships of SOM coverage and connectivity with particle sizes in the mature soil stage shows that larger particles of >10  $\mu$ m<sup>2</sup> with >15 % coverage were mainly recovered in the light fraction. Along with the increased recovery of particles in the light fraction over time, the mean particle size decreased in the light clay-sized fraction and increased in the heavy fraction (Fig. 3a, b). This suggests that fine particles were preferentially recovered in the light fraction, whereas larger particles residually enriched in the heavy fraction. This is explained by the fact, that for some fine particles, even small amounts of associated SOM were enough to be recovered in the light fraction, whereas larger particles of  $>5 \,\mu\text{m}^2$  needed higher SOM coverage for that. The heterogeneity of the particle size classes within the density fractions of the mature soil indicate a broad spectrum of formed microaggregate sizes. The building of small organo-mineral associations into larger aggregates, therefore, acts at multiple size scales from submicron to several 10 µm.

The SOM connectivity increased from 0.15 to 0.73 in the light clay-sized fraction (Fig. 5). This indicates that the SOM coatings were distributed in a patchy pattern in the beginning and grew connected to each other over time in this fraction. In contrast, the SOM connectivity in the heavy clay-sized fraction was higher and more connected than in the light fraction at 15 years after glacial retreat (Fig. 5). This could be related to the fact that at this young stage only few SOM coatings were associated with mineral particles, resulting in a high connectivity, the extreme being a single SOM coating causing a connectivity of 1. Over time after glacial retreat, the SOM connectivity in the heavy fraction decreased from 0.43 to 0.25 (Fig. 5a). In the heavy fraction, SOM coverage and connectivity showed a contrary relationship, whereas both increased in the light fraction (Fig. 4, 5). This was This article is protected by copyright. All rights reserved.

probably caused by an accumulation of residual particles in the heavy fraction with a more patchy distribution of SOM coatings, whereas those particles on which the SOM coatings grew more connected were recovered in the light fraction.

#### Development of C and N composition of soil organic matter coatings

The element distributions of the SOM coatings point to changes in the stoichiometric properties of C and N composition during the soil formation after glacial retreat. In the establishing light claysized fraction, the SOM coatings retained more N within several decades from young (15 years) to the intermediate soil (75 years) and decreased below the initial ratio from the old (111 years) to the mature site (>700 years) (Fig. 6b). This means that the SOM coatings in the light clay-sized fraction rapidly gained more N within several decades, whereas after several centuries, they gained comparatively more C. Such development possibly indicates a change of the chemical composition of SOM from aliphatic compounds to more proteinaceous ones, as reported for increasing amounts of microbial-derived SOM in earlier works (Dümig et al., 2012; Schurig et al., 2013; Sollins et al., 2009). For the primary ecosystem succession in the forefield of the Damma glacier, the highest abundance of N fixing microbes in the bulk soil and the highest N fixation activity in rhizospheres were described 75 years after glacial retreat at the intermediate stage (Brankatschk et al., 2011; Duc et al., 2009; Zumsteg et al., 2012). At the later stages of soil development, nitrate reducers and decomposers of plant-derived substrate were reported to have increased and outcompeted earlier bacteria (Zumsteg et al., 2012). This process probably also influenced the decrease of CN:C ratios of SOM coatings in the light clay-sized fraction at the mature soil stage compared to earlier stages in our study (Fig. 6b). Our direct observations of the spatial complexity and the element distributions on the coatings agree with the microbial development at the bulk scale (Schulz et al., 2013).

In the heavy clay-sized fraction, the SOM coatings mostly retained more N if they were larger (Fig. 6a). In contrast, the CN:C ratio in the light clay-sized fraction remained at similar ranges at all evaluated coating sizes (Fig. 6b). This means that the rapid growth of the SOM coatings over time probably mediates more N-rich SOM coatings with a certain extent. This is confirmed by the higher This article is protected by copyright. All rights reserved.

C:N ratios at bulk scale and higher CN:C ratios at microscale when comparing the light clay-sized fraction and its larger SOM coatings with the heavy fraction at all development stages (Table 1, Fig. 6). This means that the N-rich SOM, which mostly derive from microbes, increased hand in hand with the evolving light clay-sized fraction, showing that microbes play an active role in the formation of soil microstructures.

In conclusion, our results reveal that SOM accrual drives the initial formation of soil structure over time after glacial retreat. We summarized the successive patterns of soil structure formation in a schematic overview shown in Fig. 7. The initial soil formation in ecosystems triggered by a changing climate showed a rapid development of soil microaggregates at a decadal timescale that may sequester soil organic matter for the long-term. We found SOM coatings at the microscale that increasingly covered the mineral surfaces over time. The SOM coatings grew over time and developed from patchy-distributed to more connected SOM coatings. The growth of already existing SOM coatings means that the adsorptive mineral surface is a poor estimate of the limit of SOM sequestration potential of soils. Instead, the association of SOM on mineral surfaces is governed by sorptive properties of both organic and mineral surfaces and their spatial interactions at microscale. We observed that the SOM accrual was dominated by a growth of SOM coatings at the mineral surfaces and not limited by the slow development of fresh mineral surfaces provided by geochemical weathering. After a rapid increase in the beginning, the rate of SOM coverage became lower after several centuries. This means that in mature soils the SOM accrual on mineral surfaces does not mask their surface properties. Instead, the SOM adds to the functionality of mineral surfaces and together they provide soil functions such as the biogeochemical cycling of carbon, nutrients, and water. The retention of N-rich SOM rapidly increased after several decades, whereas it changed to SOM that is richer in carbon than in the initial soils after some centuries. These stoichiometric changes of the SOM coatings over time after glacial retreat agree with the reported N dynamics of primary ecosystem succession in earlier works at the same site. According to the comparable net carbon input at Damma and other glaciers (Dümig et al., 2011; Smittenberg et al., 2012), we assume that the observed successive patterns of microspatial SOM accrual may also be valid for other alpine This article is protected by copyright. All rights reserved.

and polar ecosystems with initial soil formation. The potential decoupling of SOM accrual from mineral surface properties and their heterogeneous spatial dynamics at the microscale describe important mechanisms of SOM sequestration in soils affected by a changing climate.

# Acknowledgments

We thank Maria Greiner, Johann Lugmeier and Alexander Dümig for their technical assistance and provision of the samples. We acknowledge the financial support by the Deutsche Forschungsgemeinschaft within the framework of the research unit "MAD Soil - Microaggregates: Formation and turnover of the structural building blocks of soils" (DFG RU 2179) through project KO 1035/48-1 and for the NanoSIMS instrument (KO 1035/38-1).

# References

- Alleon J, Bernard S, Remusat L, Robert F (2015) Estimation of nitrogen-to-carbon ratios of organics and carbon materials at the submicrometer scale. Carbon, **84**, 290-298.
- Anderson SP (2007) Biogeochemistry of glacial landscape systems. In: *Annual Review of Earth and Planetary Sciences.* pp 375-399.
- Bernasconi SM, Bauder A, Bourdon B *et al.* (2011) Chemical and Biological Gradients along the Damma Glacier Soil Chronosequence, Switzerland. Vadose Zone Journal, **10**, 867.
- Bradley JA, Singarayer JS, Anesio AM (2014) Microbial community dynamics in the forefield of glaciers. Proceedings of the Royal Society B: Biological Sciences, **281**.
- Brankatschk R, Towe S, Kleineidam K, Schloter M, Zeyer J (2011) Abundances and potential activities of nitrogen cycling microbial communities along a chronosequence of a glacier forefield. ISME J, **5**, 1025-1037.
- Chenu C, Plante AF (2006) Clay-sized organo-mineral complexes in a cultivation chronosequence: revisiting the concept of the 'primary organo-mineral complex'. European Journal of Soil Science, 57, 596-607.
- Chenu C, Stotzky G (2002) Interactions between microorganisms and soil particles: an overview. In: *In Interactions between Soil Particles and Microorganisms: Impact on the Terrestrial Ecosystem.* (eds Huang PM, Bollag JM, Senesi N) pp 3-40. USA, John Wiley and Sons.
- Conant RT, Ryan MG, Ågren GI *et al.* (2011) Temperature and soil organic matter decomposition rates synthesis of current knowledge and a way forward. Global Change Biology, **17**, 3392-3404.
- Conen F, Yakutin MV, Zumbrunn T, Leifeld J (2007) Organic carbon and microbial biomass in two soil development chronosequences following glacial retreat. European Journal of Soil Science, 58, 758-762.
- Dignac MF, Derrien D, Barré P *et al.* (2017) Increasing soil carbon storage: mechanisms, effects of agricultural practices and proxies. A review. Agronomy for Sustainable Development, **37**.
- Duc L, Noll M, Meier BE, Bürgmann H, Zeyer J (2009) High Diversity of Diazotrophs in the Forefield of a Receding Alpine Glacier. Microbial Ecology, **57**, 179-190.
- Dümig A, Häusler W, Steffens M, Kögel-Knabner I (2012) Clay fractions from a soil chronosequence after glacier retreat reveal the initial evolution of organo–mineral associations. Geochimica et Cosmochimica Acta, **85**, 1-18.

- Dümig A, Smittenberg R, Kögel-Knabner I (2011) Concurrent evolution of organic and mineral components during initial soil development after retreat of the Damma glacier, Switzerland. Geoderma, **163**, 83-94.
- Egli M, Mavris C, Mirabella A, Giaccai D (2010) Soil organic matter formation along a chronosequence in the Morteratsch proglacial area (Upper Engadine, Switzerland). Catena, **82**, 61-69.
- Ernakovich JG, Hopping KA, Berdanier AB, Simpson RT, Kachergis EJ, Steltzer H, Wallenstein MD (2014) Predicted responses of arctic and alpine ecosystems to altered seasonality under climate change. Global Change Biology, **20**, 3256-3269.
- Esperschütz J, Welzl G, Schreiner K, Buegger F, Munch JC, Schloter M (2011) Incorporation of carbon from decomposing litter of two pioneer plant species into microbial communities of the detritusphere. FEMS Microbiology Letters, **320**, 48-55.
- Gibbs MT, Kump LR (1994) Global chemical erosion during the Last Glacial Maximum and the present: Sensitivity to changes in lithology and hydrology. Paleoceanography, **9**, 529-543.
- Göransson H, Welc M, Bünemann EK, Christl I, Venterink HO (2016) Nitrogen and phosphorus availability at early stages of soil development in the Damma glacier forefield, Switzerland; implications for establishment of N2-fixing plants. Plant and Soil, **404**, 251-261.
- Gormanns P, Reckow S, Poczatek JC, Turck CW, Lechene C (2012) Segmentation of Multi-Isotope Imaging Mass Spectrometry Data for Semi-Automatic Detection of Regions of Interest. PLoS ONE, 7, e30576.
- Grundmann GL (2004) Spatial scales of soil bacterial diversity The size of a clone. FEMS Microbiology Ecology, **48**, 119-127.
- Haeberli W, Beniston M (1998) Climate change and its impacts on glaciers and permafrost in the Alps. Ambio, **27**, 258-265.
- Hämmerli A, Waldhuber S, Miniaci C, Zeyer J, Bunge M (2007) Local expansion and selection of soil bacteria in a glacier forefield. European Journal of Soil Science, **58**, 1437-1445.
- Hatton P-J, Remusat L, Zeller B, Derrien D (2012) A multi-scale approach to determine accurate elemental and isotopic ratios by nano-scale secondary ion mass spectrometry imaging. Rapid Communications in Mass Spectrometry, **26**, 1363-1371.
- He L, Tang Y (2008) Soil development along primary succession sequences on moraines of Hailuogou Glacier, Gongga Mountain, Sichuan, China. Catena, **72**, 259-269.
- Herrmann AM, Ritz K, Nunan N *et al.* (2007) Nano-scale secondary ion mass spectrometry A new analytical tool in biogeochemistry and soil ecology: A review article. Soil Biology and Biochemistry, **39**, 1835-1850.
- Huggett RJ (1998) Soil chronosequences, soil development, and soil evolution: A critical review. Catena, **32**, 155-172.
- Kaiser K, Guggenberger G (2007) Sorptive stabilization of organic matter by microporous goethite: Sorption into small pores vs. surface complexation. European Journal of Soil Science, **58**, 45-59.
- Keusen HR, Ganguin J, Schuler P, Buletti M (1989) *Felslabor Grimsel, Geologie,* Technischer Bericht 87-14, Baden, Switzerland, NAGRA.
- Kiczka M, Wiederhold JG, Frommer J, Voegelin A, Kraemer SM, Bourdon B, Kretzschmar R (2011) Iron speciation and isotope fractionation during silicate weathering and soil formation in an alpine glacier forefield chronosequence. Geochimica et Cosmochimica Acta, 75, 5559-5573.
- Kim H, Nunan N, Dechesne A, Juarez S, Grundmann G (2015) The spatial distribution of exoenzyme activities across the soil micro-landscape, as measured in micro- and macro-aggregates, and ecosystem processes. Soil Biology and Biochemistry, **91**, 258-267.
- Kleber M, Eusterhues K, Keiluweit M, Mikutta C, Mikutta R, Nico PS (2015) Mineral–Organic Associations: Formation, Properties, and Relevance in Soil Environments. Advances in Agronomy, 130, 1-140.
- Kögel-Knabner I, Guggenberger G, Kleber M *et al.* (2008) Organo-mineral associations in temperate soils: Integrating biology, mineralogy, and organic matter chemistry. Journal of Plant Nutrition and Soil Science, **171**, 61-82.
- Konert M, Vandenberghe JEF (1997) Comparison of laser grain size analysis with pipette and sieve analysis: a solution for the underestimation of the clay fraction. Sedimentology, **44**, 523-535.

- Lindeberg T (1998) Feature Detection with Automatic Scale Selection. International Journal of Computer Vision, **30**, 79-116.
- Mueller CW, Kölbl A, Hoeschen C, Hillion F, Heister K, Herrmann AM, Kögel-Knabner I (2012) Submicron scale imaging of soil organic matter dynamics using NanoSIMS – From single particles to intact aggregates. Organic Geochemistry, **42**, 1476-1488.
- Mueller CW, Weber PK, Kilburn MR, Hoeschen C, Kleber M, Pett-Ridge J (2013) Advances in the Analysis of Biogeochemical Interfaces: NanoSIMS to Investigate Soil Microenvironments. Advances in Agronomy, **121**, 1-46.
- Nunan N, Young IM, Crawford JW, Ritz K (2007) Bacterial interactions at the microscale Linking habitat to function in soil. In: *The Spatial Distribution of Microbes in the Environment*. (eds Franklin RB, Mills AL) pp 61-85.
- Ollivier J, Töwe S, Bannert A *et al.* (2011) Nitrogen turnover in soil and global change. FEMS Microbiology Ecology, **78**, 3-16.
- Pallud C, Dechesne A, Gaudet JP, Debouzie D, Grundmann GL (2004) Modification of spatial distribution of 2,4-dichlorophenoxyacetic acid degrader microhabitats during growth in soil columns. Applied and Environmental Microbiology, **70**, 2709-2716.
- Pronk GJ, Heister K, Ding G-C, Smalla K, Kögel-Knabner I (2012) Development of biogeochemical interfaces in an artificial soil incubation experiment; aggregation and formation of organo-mineral associations. Geoderma, **189-190**, 585-594.
- Remusat L, Hatton PJ, Nico PS, Zeller B, Kleber M, Derrien D (2012) NanoSIMS study of organic matter associated with soil aggregates: advantages, limitations, and combination with STXM. Environ Sci Technol, 46, 3943-3949.
- Renard P, Allard D (2013) Connectivity metrics for subsurface flow and transport. Advances in Water Resources, **51**, 168-196.
- Rennert T, Totsche KU, Heister K, Kersten M, Thieme J (2012) Advanced spectroscopic, microscopic, and tomographic characterization techniques to study biogeochemical interfaces in soil. Journal of Soils and Sediments, **12**, 3-23.

RStudio Team (2015): Integrated Development Environment for R. Boston, USA, RStudio, Inc.

Schaltegger U (1990) The Central Aar granite: highly differentiated calc-alkaline magmatism in the Aar Massif (central Alps, Switzerland). European Journal of Mineralogy, **2**, 245-259.

- Schindelin J, Rueden CT, Hiner MC, Eliceiri KW (2015) The ImageJ ecosystem: An open platform for biomedical image analysis. Molecular Reproduction and Development, **82**, 518-529.
- Schlüter S, Sheppard A, Brown K, Wildenschild D (2014) Image processing of multiphase images obtained via X-ray microtomography: A review. Water Resources Research, **50**, 3615-3639.
- Schmidt SK, Reed SC, Nemergut DR *et al.* (2008) The earliest stages of ecosystem succession in highelevation (5000 metres above sea level), recently deglaciated soils. Proceedings of the Royal Society B: Biological Sciences, **275**, 2793-2802.
- Schulz S, Brankatschk R, Dümig A, Kögel-Knabner I, Schloter M, Zeyer J (2013) The role of microorganisms at different stages of ecosystem development for soil formation. Biogeosciences, 10, 3983-3996.
- Schumaker NH (1996) Using landscape indices to predict habitat connectivity. Ecology, **77**, 1210-1225.
- Schurig C, Smittenberg RH, Berger J *et al.* (2013) Microbial cell-envelope fragments and the formation of soil organic matter: A case study from a glacier forefield. Biogeochemistry, **113**, 595-612.
- Smittenberg RH, Gierga M, Göransson H, Christl I, Farinotti D, Bernasconi SM (2012) Climate-sensitive ecosystem carbon dynamics along the soil chronosequence of the Damma glacier forefield, Switzerland. Global Change Biology, **18**, 1941-1955.
- Sollins P, Kramer MG, Swanston C *et al.* (2009) Sequential density fractionation across soils of contrasting mineralogy: evidence for both microbial- and mineral-controlled soil organic matter stabilization. Biogeochemistry, **96**, 209-231.
- Sollins P, Swanston C, Kleber M *et al.* (2006) Organic C and N stabilization in a forest soil: Evidence from sequential density fractionation. Soil Biology and Biochemistry, **38**, 3313-3324.
  Sommer C, Strähle C, Köthe U, Hamprecht FA (2011) ilastik: Interactive Learning and Segmentation

Toolkit. In: *Eighth IEEE International Symposium on Biomedical Imaging (ISBI).* pp 230-233. Totsche KU, Amelung W, Gerzabek MH *et al.* (2018) Microaggregates in soils. Journal of Plant Nutrition and Soil Science.

- Tscherko D, Hammesfahr U, Marx M-C, Kandeler E (2004) Shifts in rhizosphere microbial communities and enzyme activity of Poa alpina across an alpine chronosequence. Soil Biology and Biochemistry, **36**, 1685-1698.
- Vogel C, Mueller CW, Hoschen C *et al.* (2014) Submicron structures provide preferential spots for carbon and nitrogen sequestration in soils. Nature Communication, **5**, 2947.
- Von Lützow M, Kögel-Knabner I, Ekschmitt K, Matzner E, Guggenberger G, Marschner B, Flessa H (2006) Stabilization of organic matter in temperate soils: Mechanisms and their relevance under different soil conditions - A review. European Journal of Soil Science, 57, 426-445.
- Wagai R, Mayer LM, Kitayama K (2009) Extent and nature of organic coverage of soil mineral surfaces assessed by a gas sorption approach. Geoderma, **149**, 152-160.
- Walker LR, Wardle DA, Bardgett RD, Clarkson BD (2010) The use of chronosequences in studies of ecological succession and soil development. Journal of Ecology, **98**, 725-736.
- Yang XM, Drury CF, Reynolds WD, Yang JY (2016) How do changes in bulk soil organic carbon content affect carbon concentrations in individual soil particle fractions? Scientific Reports, **6**.
- Zemp M, Haeberli W, Hoelzle M, Paul F (2006) Alpine glaciers to disappear within decades? Geophysical Research Letters, **33**.
- Zumsteg A, Luster J, Göransson H *et al.* (2012) Bacterial, Archaeal and Fungal Succession in the Forefield of a Receding Glacier. Microbial Ecology, **63**, 552-564.

# Tables

**Table 1** Properties of organic matter in the clay-sized fraction (<2  $\mu$ m; n = 2) and its heavy (>2.2 g cm<sup>-3</sup>) and light subfraction (1.6-2.2 g cm<sup>-3</sup>).

Develop- ment stage	Years after glacial retrea t	SOC (mg g <sup>-1</sup> )			N (mg g <sup>-1</sup> )			C:N			Clay content <sup>a</sup>
		Clay <sup>a</sup>	Heavy clay	Light clay	Clay <sup>a</sup>	Heavy clay	Light clay	Clay <sup>a</sup>	Heavy clay	Light clay	(% of bulk soil)
Young	15	44.4	32.4	153	4.9	3.7	11.4	9	9	13	3
Intermediat	71	232.7	59.1	197.1	22	7.1	17.4	11	8	11	4
е	79	193.7	63.9	144.3	19.5	6.9	13.1	10	9	11	13
Old	111	197.2	81.6	178.7	19.9	7.8	16.5	10	10	11	4
Mature	>700	330.9	38.3	335.5	24	4.2	23.4	14	9	14	7
SOC, soil organic carbon; N, total nitrogen; C:N, carbon to nitrogen ratio; <sup>a</sup> , data adapted from Dümig et al. (2012).											

# **Figure captions**

**Fig. 1** (a) Mass recovery of heavy (>2.2 g cm<sup>-3</sup>) and light (1.6-2.2 g cm<sup>-3</sup>) clay-sized density fraction from bulk soil over time after retreat of the Damma glacier. (b) SOC in the clay-sized fractions normalized to the bulk soil.

**Fig. 2** Example measurements at the microscale showing (a, b, c) Scanning electron microscopy image and composite images of NanoSIMS measurements with secondary ion counts of (d, e, f) <sup>16</sup>O<sup>-</sup>, (g, h, i) <sup>12</sup>C<sup>-</sup>, and (j, k, l) <sup>12</sup>C<sup>14</sup>N<sup>-</sup> as a heat map. (m, n, o). Above the grayscale <sup>16</sup>O<sup>-</sup> distribution, the normalized CN:C ratio ( ${}^{12}C^{14}N^{-}$ : ( ${}^{12}C^{14}N^{-} + {}^{12}C^{-}$ )) of SOM coatings is shown as a heat map. Scale bar is 5 µm.

**Fig. 3** Frequency distribution and mean size of various size classes and mean size of particles in the Damma glacier forefield at various times after glacial retreat according to the image analysis of NanoSIMS measurements in (a) a heavy clay-sized fraction >2.2 g cm<sup>-3</sup> (triangles) and (b) a light clay-sized fraction 1.6-2.2 g cm<sup>-3</sup> (circles). The frequency distribution and size of SOM coatings is shown in (c) a heavy clay-sized fraction >2.2 g cm<sup>-3</sup> (triangles) and (d) a light clay–sized fraction 1.6-2.2 g cm<sup>-3</sup> (circles). The scale of the right y-axis in (a, b) is ten times the one in (c, d). The soil This article is protected by copyright. All rights reserved.

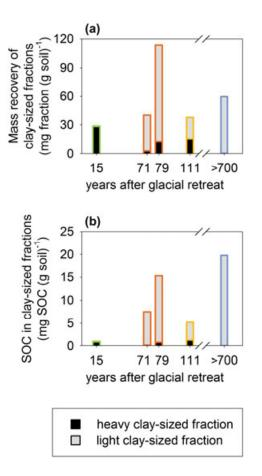
chronosequence comprised several stages of soil development: young (green), intermediate (orange), old (yellow), and a mature site (blue). The symbols display arithmetic means, and the error bars denote standard errors. The ANOVAs were statistically significant (p<0.001), and means with the same letter and case do not differ significantly (Tukey's HSD).

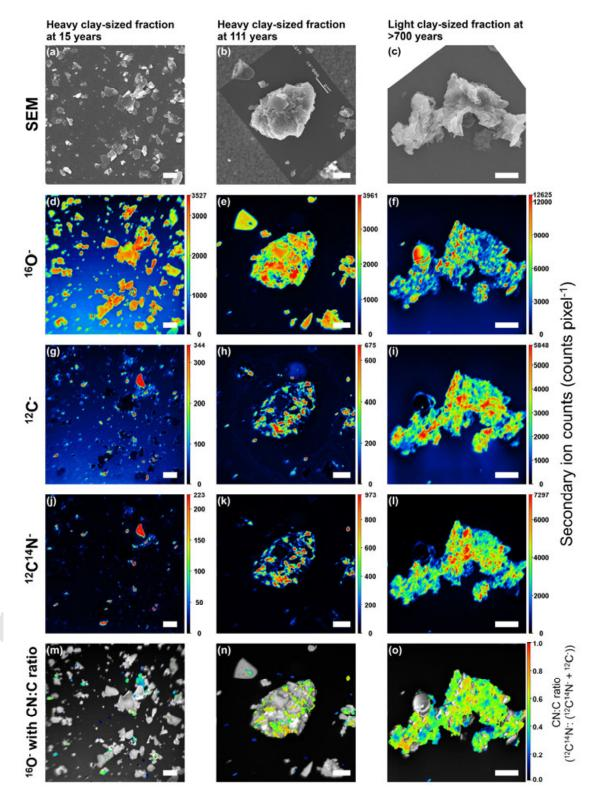
**Fig. 4** The degree of SOM coverage in the Damma glacier forefield after deglaciation based on image analysis of NanoSIMS measurements in (a) the heavy clay-sized fraction >2.2 g cm<sup>-3</sup> (triangles) and (b) the light clay-sized fraction 1.6-2.2 g cm<sup>-3</sup> (circles). The soil chronosequence comprised several stages of soil development: young (green), intermediate (orange), old (yellow), and a mature reference site (blue). The symbols and bars display the summed area of the SOM area divided by the summed area of the particle area (Equation 1).

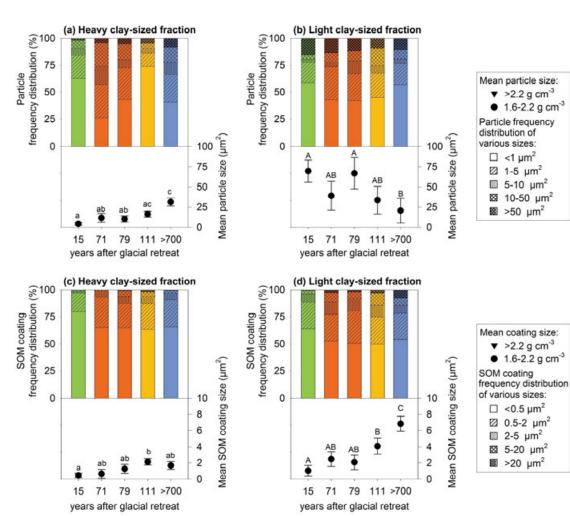
**Fig. 5** The connectivity of SOM coatings in the Damma glacier forefield after deglaciation based on an image analysis of NanoSIMS measurements in (a) the heavy clay-sized fraction >2.2 g cm<sup>-3</sup> (triangles) and (b) the light clay-sized fraction 1.6-2.2 g cm<sup>-3</sup> (circles). The soil chronosequence comprised several stages of soil development: young (green), intermediate (orange), old (yellow), and a mature reference site (blue). The symbols and bars display area-weighted means (Equation 2 and 3).

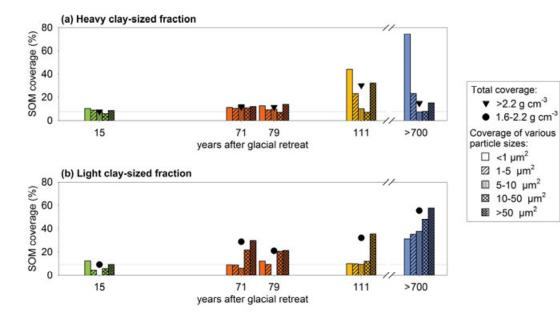
**Fig. 6** Normalized CN:C ratio ( ${}^{12}C^{14}N^-$ : ( ${}^{12}C^{14}N^-$  +  ${}^{12}C^-$ )) of SOM coatings in (a) the heavy clay-sized fraction >2.2 g cm<sup>-3</sup> (triangles) and (b) the light clay-sized fraction 1.6-2.2 g cm<sup>-3</sup> (circles) of developing soils in the Damma glacier forefield with different times after glacial retreat. The bars and symbols display arithmetic means, and the error bars denote standard errors. The ANOVAs were statistically significant (p<0.001), and means with the same letter and case do not differ significantly (Tukey's HSD).

**Fig. 7** Schematic overview of the initial soil structure formation over time after retreat of the Damma glacier. The light clay-sized fraction 1.6-2.2 g cm<sup>-3</sup> (blue line) increased at the expense of the heavy clay-sized fraction >2.2 g cm<sup>-3</sup> (pink line). The composite images of NanoSIMS measurements show representative spots according to the total SOM coverage, area-weighted SOM connectivity, and the arithmetic mean particle size with a 5  $\mu$ m scale bar. "Hollow" particles in the <sup>16</sup>O<sup>-</sup> distribution indicate charging effects occurring on soil minerals not covered with SOM coatings and were classified as mineral surfaces.







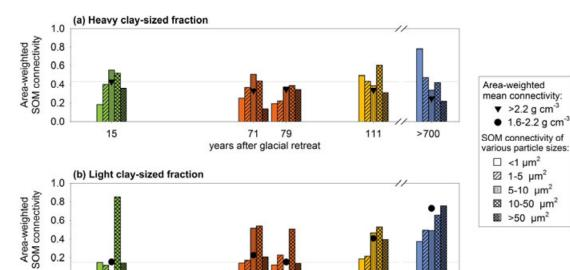


0.4 0.2

0.0

0

15



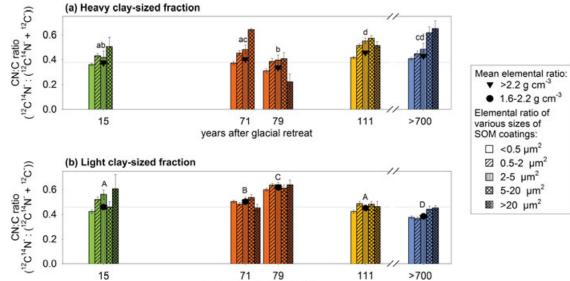
71

years after glacial retreat

79

111

>700



years after glacial retreat

 $2-5 \ \mu m^2$ 

Contribution of<br/>light fraction<br/>(1.6-2.2 g cm-3)SOC conc. in<br/>density fractionParticle sizeSOM coating<br/>sizeSOM coverage<br/>on mineral<br/>surfacesSOM<br/>connectivity

CN:C ratio of SOM coatings

Representative particles of the heavy fraction in NanoSIMS

Representative particles of the light fraction in NanoSIMS

